# A Novel LISS-III Swath Extension through Wider AWiFS Swath and SVM Training and Learning

Radhika Kammili[1], Venkateswara Rao Chandu[2], Kamakshi Prasad Valurouthu[3]

[1] DMS SVH College of Engineering, Machilipatnam, India.
Email: kammilisrr@gmail.com
[2] National Remote Sensing Centre, Hyderabad, India.
[3] JNTUH, Hyderabad, India

***Abstract* - In the process of acquiring wider swath images, space borne sensors cannot offer simultaneous high spatial and temporal resolutions. Our project deals with an original technique of processing and using images of two on-board sensors viz., Resourcesat-1 (RS1) LISS-III (High Resolution HR) combined with AWiFS (Low Resolution LR) wider swath data to provide high spatial and temporal resolutions simultaneously. While 23x23m+24 days pertains to the Spatial Resolution (SR)+Temporal Resolution (TR) of LISS-III, 56x56m+5 days correspond to the SR+TR of AWiFS respectively. In the process of acquisition at the same time, the LISS-III swath 140km coincides at the exact centre region of 740km swath of AWiFS. If the non-overlapping area of AWiFS has the same features of Earth's surface as of HR overlapping area, it then provides a way to increase SR of AWiFS to SR of LISS-III in the same non-overlapping area. Knowing this, a novel processing technique is proposed to improve the SR of LISS-III in non-overlapping area using Single-Image Super-Resolution (SISR) technique with Support Vector Machine (SVM) learning and training methods applied on the data sets. The proposed technique results in an image having 740km swath at SR of 23x23m and TR of 5 days. We demonstrate the quality of our method using experimental results in terms of prediction accuracy assessment parameters.**

***Keywords - Support Vector Machine training and learning, Spatial Resolution, Temporal Resolution, Swath, AWiFS-LISS-III sensors, Single-Image Super-resolution.***

## I. INTRODUCTION

For accurate follow up of agriculture, spatial as well as temporal changes of crops have to be closely monitored. This is important for decision making systems aimed at agricultural application [1]. During monsoon, agricultural lands are very much affected by floods [2]. Prediction of floods in advance, monitoring of natural hazards need data from wider swath, say for example, high TR and high SR data from total water sheds [3]. Watershed represents a basic ecosystem and its functionality against several such systems is not an efficient assessment of environment as well as land cover [4]. Identifying different types of vegetation and habitats derivation requires high spatial data for classification of land cover [5]. Upcoming ecological and land-cover variations can be estimated by temporal studies, for example, to evaluate the outcome of anthropogenic land-use routines on protected species [4]. Wide swath images with high SR and TR are needed in several applications of remote sensing viz., accurate agriculture monitoring, prediction of floods, precision natural hazard follow up, total ecosystems and land-cover variations.

However obtaining an image data with longer swath having high SR and TR at the same instant has been a major setback with satellite remote sensing systems. Ground sampling distance and swath width are directly related and revisit time is inversely related to swath width [6]. One alternative to obtain images with wide swath, finer SR and high TR is by improving the low SR to fine SR of the image using ground processing techniques. This is possible by using SISR methods [7].

TABLE 1. RESOURCESAT-1 SATELLITE SENSORS LISS-III AND AWIFS CHARACTERISTICS

| | LISS-III | | AWiFS | |
|---|---|---|---|---|
| **Spectral Bands** | B2 | 0.52-0.59µm | B2 | 0.52-0.59µm |
| | B3 | 0.62-0.68µm | B3 | 0.62-0.68µm |
| | B4 | 0.77-0.86µm | B4 | 0.77-0.86µm |
| | B5 | 1.55-1.70µm | B5 | 1.55-1.70µm |
| **Spatial Resolution** | 23m | | 56m | |
| **Temporal Resolution** | 24 days | | 5 days | |
| **Width of Swath** | 140 km | | 740 km | |

Advanced Wide-Field Sensor (AWiFS) and Linear Imaging and Self-scanning Sensor (LISS-III) are two onboard sensors of ISRO's Resourcesat-1 Indian Satellite. For LISS-III, SR is 23x23m and for AWiFS it is 56x56m. LISS-III has temporal resolution of 24days and AWiFS has 5days. Characteristics of two sensors are given in Table1.

Figure1 shows the acquisition process of the two sensors of Resourcesat-1 satellite at the same instant. At the centre, LISS-III overlapping area of 140km swath corresponding to 740km swath of AWiFS. Smaller swath (140km) of HR image can be extended to wider swath (740km) provided same features of Earth's surface are

observed in nonoverlapping area of AWiFS and LISS-III. HR data patch and its respective AWiFS data patch in overlapped area in turn serve as priori knowledge to increase SR of nonoverlapped area by SISR technique. SISR [8-11], initially put forth by Baker and Kanade (2002), tries to obtain priori relationship used for amongst LR and HR image blocks and then uses these relationships to forecast LISS-III data from AWiFS data. SISR is put forth initially as a kernel learning concept then predicts the HR information by Support Vector Regression (SVR) [12-15].

## II. LITERATURE SURVEY

Owing to the trade-off amongst both SR and TR being high, this work includes a novel method to generate images with TR and SR both being high. Indian Remote Sensing Satellite (IRS P6), also referred as Resourcesat-1, one of ISRO's missions has on board LISS-III, LISS-IV and AWiFS. Images of these sensors vary in resolutions as well as in coverage. For LISS-III the SR is 23m and for AWiFS it is 56m. TR is 24 days for LISS-III image with 23m SR and 5-day TR. Method is dependent on the subpixel relationship existing amongst a single AWiFS : LISS-III image pair, captured prior to or after the date of prediction. Synthetic LISS-III image at time $t_k$ is predicted through AWiFS image at time $t_o$, and $t_o$ is not equal $t_k$.

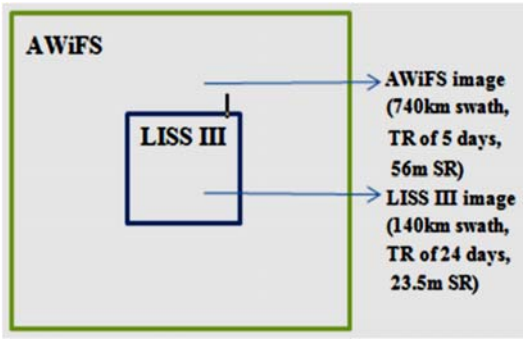


Figure 1. Cross Section of LISS-III and AWIFS

Results obtained for the proposed method proved it to be efficient in prediction accuracy terms, computational efficiency when compared to the other prevailing procedures of spatio temporal data fusion [23].

To study the radiometric calibration accuracy of IRS P6, LISS-III and AWiFS sensors, image pairs of these sensors were in turn compared with images of Landsat-5 Thematic Mapper (TM) and Landsat-7 Enhanced TM plus (ETM+) sensors. Surface observations are calibrated depending on image statistics using regions covered near simultaneously using two images. For classifying land-cover classes, LISS-III and AWiFS products are found to be less accurate but could provide more usable approximate to L7 ETM+ and L5 TM in term of other two National Land Cover Dataset (DLCD) products viz., percent impervious surface and percent tree canopy [16].

Existing RS imagery system results in great variety of spatial, temporal and spectral resolution. A single sensor's performance might not be satisfactory in the sense of SR, swath width and TR simultaneously using to its technological short comings great number of application viz., feature detection, change detection analysis, land use and land cover classification require the maximum possible resolutions and longest serving period to meet their goals. Therefore there is a need to use multi-sensor data fusion between various sensors has to be cautiously addressed for this sort of applications [21].

SVM's (Support Vector Machine) are used efficiently for classification of data. Classification procedure generally includes dividing data into training and testing groups. Each case in the set of training consists of one class label along with many features. The training data the one which could predict the targeted values corresponding to the test data when test data attributes are only given. Basic SVM uses four basic kernel viz., linear, polynomial, radial basis functions (RBF) and sigmoid [22].

Space borne sensors have limitation in capturing images with greater swath and high TR, SR at the same instant. SVM is used in predicting HR image with LR-HR pair of images for a respective LR image. This represents fusion of data using more number of sensors so as to obtain adequate information to meet the requirements aimed towards a specific application [17]. Spatio-temporal fusion is proposed for creating HSHT images by learning through one pair of priori images. Implementation involves two stages. First stage consists of improving SR of LSHT image data corresponding to priori as well as prediction dates. Second stage involves fusing the known HSLT with the super resolved LSHT's using high-pass modulation thus producing HSHT data corresponding to the prediction data [18].

"Sparse-representation-based spatio temporal reflectance Fusion Model" (SPSTFM) predicts HSR surface reflectances using data involved with LSR scenes. More specifically this model creates a unique framework involving fusion of RS images having varying temporal reflectance, phenology and type changes through establishment of correspondence amongst structures belonging to HSR images of given patches with respective LSR images [19].

For further classification, using the available training data, learning using distance metric focus to learn via a valid metric of distance, from which similarity existing amongst data samples can be much more efficiently assessed. Work formulates metric-learning as one such kernel classification issue associated with a positive semi definite constraint which is then solved using iterative training method of SVM's. Non negative-coefficient constrained-metric learning and positive semi definite constrained-metric learning are the two novel-metric

learning-models that are developed. Both methods can assume global optimality to their solutions. Face-verification along with person re-identification, general classification are used during experiments which are used to evaluate the proposed methods. In comparison with existing methods of approach, proposed work achieved considerable improvement in classification accuracy and also found to be efficient in terms of training [20].

Huber loss function within SVR has been used for estimating biophysical parameters acquired using RS data. Various forms of noise in the dataset can be handled using the above cost function method produced highly accurate and increased robust estimation results in comparison to different cost functions well within SVR framework, neural networks, bio-optical model particularly in the case of less in situ measurements being available [24].

SVM's are used for classifying Hyperspectral RS images. Performance accuracy of SVM's is compared with that of non-parametric classifiers (i.e., radial basis function neural networks and the k-nearest neighbour classifier). Multiclass strategies, one-against-all, one-against-one and hierarchical two tree-based strategies are compared after analysis. Various performance parameters viz., classification accuracy, computational time, stability of setting parameter along with complexity of multiclass architecture are used in extending support to experimental analysis in elaborate and accurate manner for classification of spectro radiometer hyperspectral data SVM's proved to be valid and robust alternative compared to conventional pattern recognition methods [25].

More advanced regression algorithms SVR, KRR (Kernel Ridge Regression), NN, RFR (Random forest regression), PLSR (Partial Least Squares Regression) synthetically mixed training data in quantification of 3.6 and 9m SR. Findings suggested that KRR and SVR kernel methods resulted in greater accuracies in mapping of complex types of urban surface types. Also models KRR and SVR demonstrated to be more stable with respective to spectral and spatial differences among two images and efficiently used much greater complexity of synthetic training mixtures in improvisation of estimates required for coarser resolution data. Also it is proved that combining SVR and KRR, Kernel-based regression methods along with synthetic mixing of training data switched well for quantification of urban land cover acquired from images of spectrometer data at numerous scales [26].

## III. LEARNING AND PREDICTION THROUGH SVM

A hypothesis space consisting of linear functions encompassed in a high dimensional feature space provides the basis for learning systems using SVM. These machines are trained using a learning algorithm obtained using optimisation theory implementing a learning bias acquired using statistical learning theory. SVM emerged to be a very robust method in several areas of applications.

A training set of inputs along with output values (lables) are supplied to the learning machine through supervised learning. Generally the inputs exist in the form of attributed vectors. With the availability of attribute vectors, finite number of hypothesis sets are possible for any problem. Out of these, most understood ones are the linear functions also also simple to apply. Several means for separating the two classes of instances for linear functions are provided through traditional statistics as well as classical neural networks along with many ways of linear function interpolation. These methods including robust iterative methods along with generalisation properties theoretical analysis will form the frame work to provide means for complex systems construction [27].

While a classifier is trained, attempts are made in maximising the performance of classification of trained data. In case classifier seems to fit to trained data very well, there will be a degradation of generalisation ability which refers to the classification ability of unknown data. This is referred as over fitting. Normally trade-off is achieved to generalization ability and training data fitting. In a two-class problem data, SVM is trained such that the direct decision function achieves maximising the generalisation ability. This involves mapping m-dimensional input space changed to l-dimensional feature space Z where $l \geq m$. Subsequently in Z, using the optimal separating hyper plane, the two classes are separated by solving the quadratic programming problem.

In input space, training data could be linearly separable. If not linearly separable, then m-dimensional input space is mapped to l-dimensional feature space where l is more higher than m. In feature space the linear separation will be improved. Consider M m-dimensional training inputs $x_i$ (i = 1,2 ,.....M) belonging to class 1 or class 2. Let the associated labels be $y_i = 1$ for class 1 and $y_i = -1$ for class 2. Assuming that these data are linearly separable, the decision function D(x) can be determined [28].

$$D(x) = W^T x+b \quad (1)$$

Where b : bias ,
w :'m' dimensional vector.

$$W^T x_i +b= \begin{cases} <0 \text{ for } y_i = -1 \\ >0 \text{ for } y_i =1 \end{cases} \quad (2)$$

As the training data are linearly separable, no training data satisfies $W^T x + b = 0$. So to have control over separability, equation 2 is modified as following in equalities.

$$W^T x_i +b = \begin{cases} \geq = 1 \text{ for } y_i = 1 \\ \leq = -1 \text{ for } y_i = -1 \end{cases} \quad (3)$$

1 and -1 on the right hand side of the inequalities are constants a(>0) and –a respectively. When both sides of the inequalities are divided by 'a', equation 3 is the result [28].

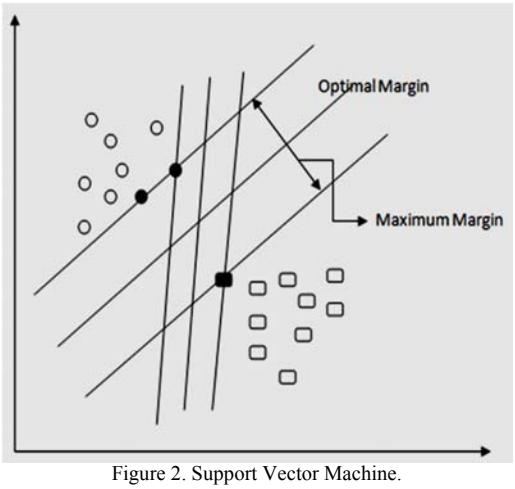


Figure 2. Support Vector Machine.

## IV. QUALITY ASSESSMENT

Comparison between original HR and Predicted HR image is done through quality assessment. RMSE, Root Mean Square Error is used for quantitative Assessment. Average Correlation Coefficient (CC), Erreue-Relative-Globale-Adimensionelle-desynthese(ERGAS) and SAM (Spectral Angle Mapper) are used to find spectral quality of synthetic images. SAM values close to zero represent less spectral distortion. Visual quality can be computed using Structural Similarity Index Map (SSIM). Prediction accuracy is computed using coefficient of determination $R^2$.

### *A. Structural Similarity Index Map*

SSIM is the similarity value between two images calculated using correlation, contrast and luminance.

$$\text{SSIM}(A_i, B_i) = \left[\frac{2\mu_{A_i}\mu_{B_i}+C_1}{\mu_{A_i}^2+\mu_{B_i}^2}\right]\cdot\left[\frac{2\sigma_{A_i}\sigma_{B_i}+C_2}{\sigma_{A_i}^2\sigma_{B_i}^2+C_2}\right]\cdot\left[\frac{\sigma_{A_iB_i}+C_3}{\sigma_{A_i}\sigma_{B_i}+C_3}\right]$$

where –

$\mu_{A_i}$ and $\mu_{B_i}$ : local sample standard derivation means of $A_i$, $B_i$ respectively,

$\sigma_{A_i}$ , $\sigma_{B_i}$ : local sample standard derivation means of $A_i$, $B_i$ respectively,

$\sigma_{A_iB_i}$ : Sample cross correlation of $A_i$ & $B_i$ after their means are removed,

$C_1$, $C_2$ & $C_3$ : Small positive constants stabilize each term [30].

### *B. Spectral Angle Mapper*

Several similarity measures were developed for spectral consistency assessment. Popular ones are SAM representing the angle between two vectors.

$$\theta\,(r, f) = \cos^{-1}\left[\frac{\sum_{i=1}^{k} r_i f_i}{\sqrt{\sum_{i=1}^{k} r_i^2 \quad \sum_{i=1}^{k} f_i^2}}\right]$$

where -

f and r : two vectors generated by the value of spectral channels near the same pixel in reference image (A) and fused image (B),

k : number of bands.

### *C. Erreue - Relative - Globale - Adimensionelle - Desynthese*

For multispectral images a similarity measure which depends on Mean Square Error estimator.

$$\text{ERGAS} = 100\,\frac{h}{l}\sqrt{\frac{l}{k}\sum_{i=1}^{k}\frac{\text{RMSE}(A_iB_i)^2}{\mu_{Ai}^2}}$$

where -

$A_i$, $B_i$ : compared bands in multispectral image,

RMSE: root mean squared euro,

$\mu_{A_i}$ : mean value of $A_i$,

K : number of bands,

$\frac{h}{l}$ : resolution images ratio.

### *D. Correlation Coefficient*

Band wise correlation is applied between reference LISS-III image and fused image to calculate the measure of similarity between them. CC is calculated using the formula.

$$r = \frac{\sum (x_i - \bar{X})^*(y_i - \bar{Y})}{\sqrt{\sum (x_i - \bar{X})^2 \sum (y_i - \bar{Y})^2}}$$

where -

r : correlation coefficient lies between -1 and +1,

r = +1: indicates complete positive correlation if x and y increases together (positive slope) in a straight line,

$\bar{X}, \bar{Y}$ : mean of $x_i$ and $y_i$ respectively,

r = -1: this is the case when 'y' decreases as 'x' increases or vice versa and is "complete negative correlation",

r =0 : means that variable x and y are uncorrelated.

### *E. Root Means Square Error*

It is the RMSE at every pixel. The difference of the grey values at each pixel location of LISS-III image with the fused image for the respective bands is found. Sum of squares of all these differences is found. The square root of mean of these pixel differences represents the RMSE.

$$\text{RMSE} = \sqrt{\frac{1}{NP}\sum(A_n(i) - B_k(i))^2}$$

where -
$A_h$ : fused image,
$B_k$ : LISS-III image,
i : current pixel,
NP : number of pixels,
h and k : represent similar bands [31].

## V. METHODOLOGY

In this paper, the satellite images are acquired from Resourcesat-1 satellite which is having AWiFS sensor at high temporal and low spatial resolution and LISS-III at high spatial and low temporal resolution. Fusion of the two images can be done in order to acquire an image with TR and SR both being high. The motive of this research work is to create synthetic image with both TR and SR high with wider swath. Synthetic image can be created with swath 740km and 23m spatial resolution 5 day revisit time.

Three stages are involved in the proposed method. In the first stage the two images namely AWiFS and LISS-III are registered. The two images are considered on the same data and at the same path and row. In the second stage the overlapping area of AWiFS and LISS-III are considered at the swath of LISS-III i.e 140km width. This data is given for SVM training. In the third stage the non-overlapping area of AWiFS (i.e swath width of 740km) where there is no LISS-III along this swath is considered. The corresponding HR image with respective to the LR image of AWiFS is predicted using SVM prediction. The synthetic image obtained is with 23km spatial resolution, temporal resolution of 5days and 740km swath width. The total procedure is represented in a block diagram shown in Figure 3.

### *A. Image Registration*

Two sensor images AWiFS and LISS-III are considered for our research work. Here two images are considered on the same date at the ideal situation that can be considered because sub pixel relationship between the pixels of High Spatial Low Temporal LISS-III image and Low Spatial High Temporal AWiFS images is complex with factors: 1. With respect to the pixel change in relative satellite azimuth angle and elevation angle of sun, 2. Crop growth changes, 3. Changes of the surface of the Earth, 4. Mixed pixel response maybe there, 5. Surface reflectance of AWiFS pixels may not be homogeneous. Pixel correspondence of AWiFS and LISS-III sensor images is established by image registration. LR and HR images are registered using control point approach. HR pixel is altered during resampling process. AWiFS spatial resolution is 56m, 2x2 pixels in HR image are made equal to single pixel of HR image. Thus one-to-one correspondence is done between AWiFS and LISS-III.

### *B. SVM Training*

The two images AWiFS and LISS-III are considered in the overlapping area for SVM training. LISS-III swath exactly overlaps at the center of AWiFS swath as shown in Figure 1.

- The swath of LISS-III image is super imposed at the centre of the swath of AWiFS image in the overlapping area because there exists the data of both the images. This data is used for SVM training.
- 5x5 window is considered in overlap area of the two images. In AWiFS image, consider 5x5 patch and in LISS-III consider the center pixel of the 5x5 patch. This data is used as a record in SVM training. 5x5 patch is reshaped as 1x25 vector for the SVM training phase.
- The window resets and it moves to next pixel on the right side and continue to the end of the row. Once the window reaches the end of the row, then moves one move towards down i.e. next v row beginning.

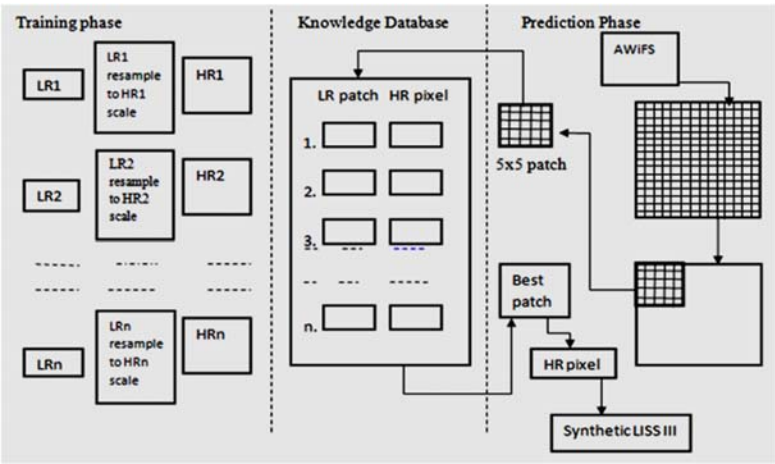


Figure 3. Block Diagram of The Methodology.

The acquired total data is given for training the knowledge using SVM training. Thus the knowledge database is created and is used for the prediction.

**Algorithm 1 Training Algorithm**

**Input:** LISS-III image: L(p, q) where p, q are overlap coordinates
AWiFS image : A(p, q) where p, q are overlap coordinates
L(p,q) and A(p, q) images are on same date and same path and same row
**Output:** Training database KDB(n) where n is (p-4)*(q-4)
**Initialise:** L(p,q) <- LISS-III image, A(p,q)<-AWiFS image
**Procedure:**

1. DB(n): R, PTH, PIX;
   a. where R: Recode number,
   b. PTH: AWiFS 5x5 path,
   c. PIX: Center pixel of LISS-III which corresponds to 5x5 path;
2. R<-1;
3. LOOP l:=1: p-4
4. LOOP n:=1: q-4
5. IF l AND m "in overlap area" THEN
   a. READ PTH <- A (l,m) [l-2 to l+2, m-2 to m+2];
   b. READ PIX <- L (l,m);
   c. DB (R)<-R, PTH,PIX;
   d. R<- R+1;
6. END IF;
7. END LOOP;
8. END LOOP;
9. KDB<-SVM-TRAIN(DB);
10. **Return** KDB;

*C. SVM Prediction*

In figure.1 the non-overlapping area of AWiFS i.e the outer box where there is no LISS-III data is given for SVM prediction to predict HR data for the corresponding AWiFS data. Objective of our research work is to improve spatial resolution of AWiFS image where there is LISS-III image. Since the Earth's surface features in the non-overlapping area may exist in the overlapping area. Such features can be predicted using SVM prediction.

- For SVM prediction the database is created for the non-overlapping area. For AWiFS image the 5x5 patch is considered as in the training phase. But for LISS-III is considered as null pixel at the centre of 5x5 patch.
- In SVM prediction also the window is moved to right of the row till row ends, and then window is moved down to next row. Thus DBI is created.
- This database is given for SVM prediction where ever similar patch is found the machine predicts a value and the remaining are left.
- The non-predicted pixels are predicted using minimum RSME . For the AWiFS 5x5 patch,the corresponding 5x5 patch with minimum RSME is found and the corresponding LISS-III pixel is predicted.

**Algorithm 2 Prediction Algorithm**

**Input:** AWiFS image : A(a,b) where a, b are nonoverlap coordinates
KDB(n) : Training database
**Output:** LISS-III Image: L(a,b) where a,b are nonoverlap coordinates.
**Initialize:** A(a,b) <- AWiFS image
L(a,b) <-0
R<-1
**Procedure:**

1. REPEAT l:=1
2. REPEAT m:=1
   a. READ PTH <- A (l,m);
   b. READ PIX <- L (l,m);
   c. DB(R)<-R, PTH,PIX;
   d. R<- R+1;
3. UNTIL l<=a-4;
4. UNTIL m<=b-4;
5. L'-> SVM-PREDICT(KDB,DB);
6. LOOP i=1 to n(DB)
7. IF PIX(i)==0 THEN
   a. PTH (x):<- COMPUTE min-RMSE(PTH(i));
   b. PIX(i)<-PIX(x);
8. END IF
9. END LOOP
10. L" <- pixels of LISS-III;
11. L(a,b) <- L'UL";
12. L(a,b) <- Total LISS-III image;

**Return** L;

With union of above two, the total LISS-III image is predicted. The image which is having 740km swath , 23m SR and 5days TR can be predicted. Finer SR image can be predicted for the coarser SR image.

## VI. EXPERIMENTAL RESULTS

In this section, the proposed method is tested on different data samples located in the southern parts of India. The data sets are considered, such that they contain different Earth's surface features like water bodies, vegetation, barren land, forest etc. The datasets used for the experiments are downloaded from BHUVAN website which belongs to National Remote Sensing Centre [29]. AWiFS and LISS-III images are downloaded on the same data of acquisition, same path and same row i.e., both

corresponds to same location. AWiFS and LISS-III images are pre-processed such that there are no differences radio-metrically, geometrically and spectrally.

Both the images are taken as same size, 500x500 pixels for experiments. For AWiFS and LISS-III images the overlapped area is taken as the square of coordinates (101, 101), (101, 400), (400,101), (400, 400). This overlap area of AWiFS and LISS-III is used for SVM training as shown in Figure 1 as inner box. The outer box is the non-overlap area i.e., the 100 pixels wide area around the inner box. Using the knowledge database obtained in the training phase is used for prediction of HR image in non-overlapping region for respective overlap region. This is done basing on the assumption that the non-overlap area may have similar earth surface features like water bodies, barren land etc in overlap area.

*A. Dataset-I*

This dataset consists of two images AWiFS and LISS-III of Resourcesat-1 satellite. Both the images are considered on same date i.e., 27 November 2009. Both the images are taken from the same area (same path and same row).

In Figure 4, 'a' represents full scene of AWiFS image. 'b' represents full scene of LISS-III image. 'c' represents the full scene of AWiFS (both the overlap and nonoverlap area) at the center overlap area of LISS-III (overlap area) is super imposed on the AWiFS image. 'd' is the predicted LISS-III image of the full scene. Figure 4 (a)-(d) are the scatter plots of the proposed method.

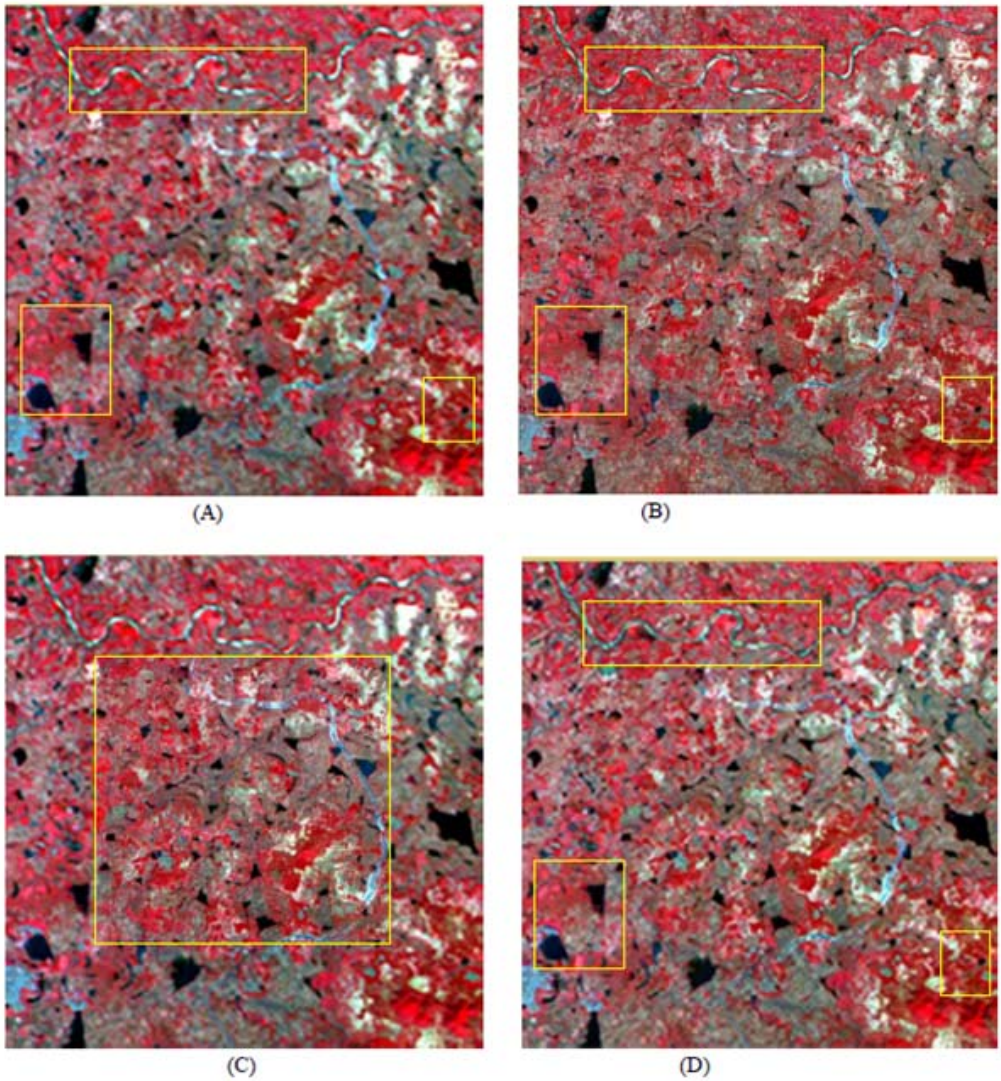


Figure 4: Synthetic LISS-III IMAGES using the Proposed Method. (A) AWiFS Image. (B) LISS-III Image. (C) LISS-III at the Centre of AWiFS. (D) Predicted Full Scene of LISS-III Image.

*B. Dataset-II*

The proposed method is also tested on another dataset which consists of set of two images LISS-III and AWiFS from Resourcesat-1 satellite. AWiFS image and LISS-III, Two images are considered on same date 31 October 2009. The images are considered of size 500x500 pixels. Both images are taken from same area, same path and same row.

In Figure 5 the results of dataset II are given. By using the proposed method the LISS-III image is predicted for the corresponding AWiFS image. Thus HR image is predicted for the corresponding LR image. Predicting the HR image in non-overlapped area using the knowledge of overlapped area. Therefore the predicted image with spatial resolution 23m, swath 740km and temporal resolution of 5 days can be predicted. Figures 6(a)-(d) shows the scatter plots of the four bands separately.

The quantitative results of our research work are shown in Table 2. The results corresponding to both the datasets are given in the below Table 2. A few of the quality assessment parameters are computed in which some of the parameters are shown band-wise and few parameters are evaluated for the multispectral image. The average RMSE of all the four band for dataset I is 4.151 and for dataset II it is 2.8231. The average SSIM for four bands for dataset I is 0.934 and for dataset II it is 0.963. The CC, ERGAS, and SAM are also shown. All these results shows the consistency of the proposed algorithms.

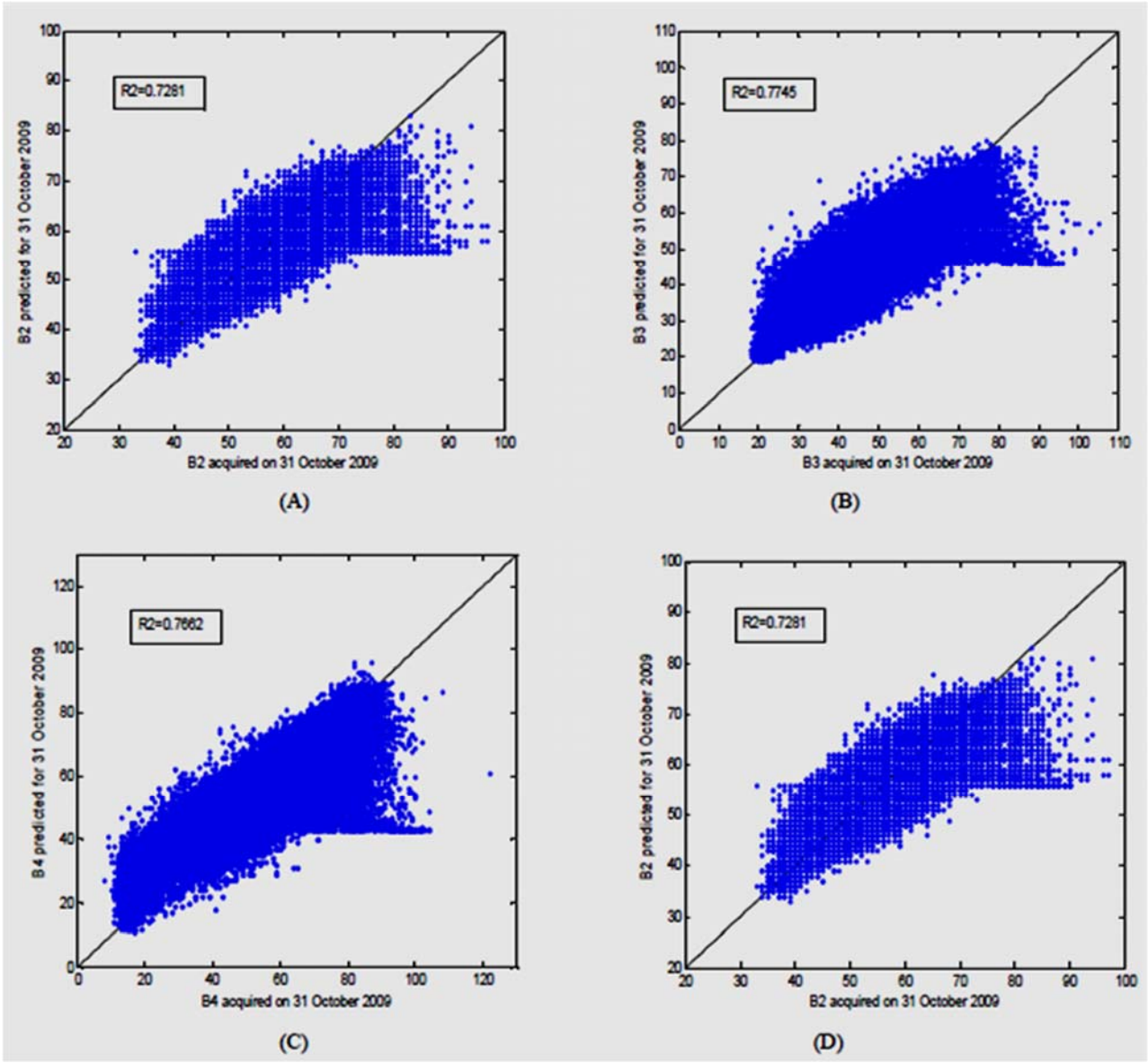


Figure 5: Scatter Plots of Four Band.

## VII. CONCLUSION

Remote sensing systems have limited capability to acquire images with high temporal, high spatial resolutions, with wide swath. Enhancement of spatial resolution along wider swath was investigated in our research work. At simultaneous acquisition of images LISS-III swath 140km overlaps with AWiFS with 740km swath at the middle portion. We assumed that non-overlapped area contains similar Earth's surface features as that of overlapped area. Assuming this, spatial resolution of AWiFS is enhanced to the spatial resolution of LISS-III in the non-overlap area. Our proposed method has maintained neighbourhood relationship among surrounding pixels, since for each pixel, surrounding patch is considered. Therefore our algorithm can create an image with high resolution 23m spatial resolution at temporal resolution 5 day at wider swath of 740km. Proposed work can be used to obtain such images. This work has been treated on two datasets and the experimental results regarding the prediction accuracy are found to be satisfactory.

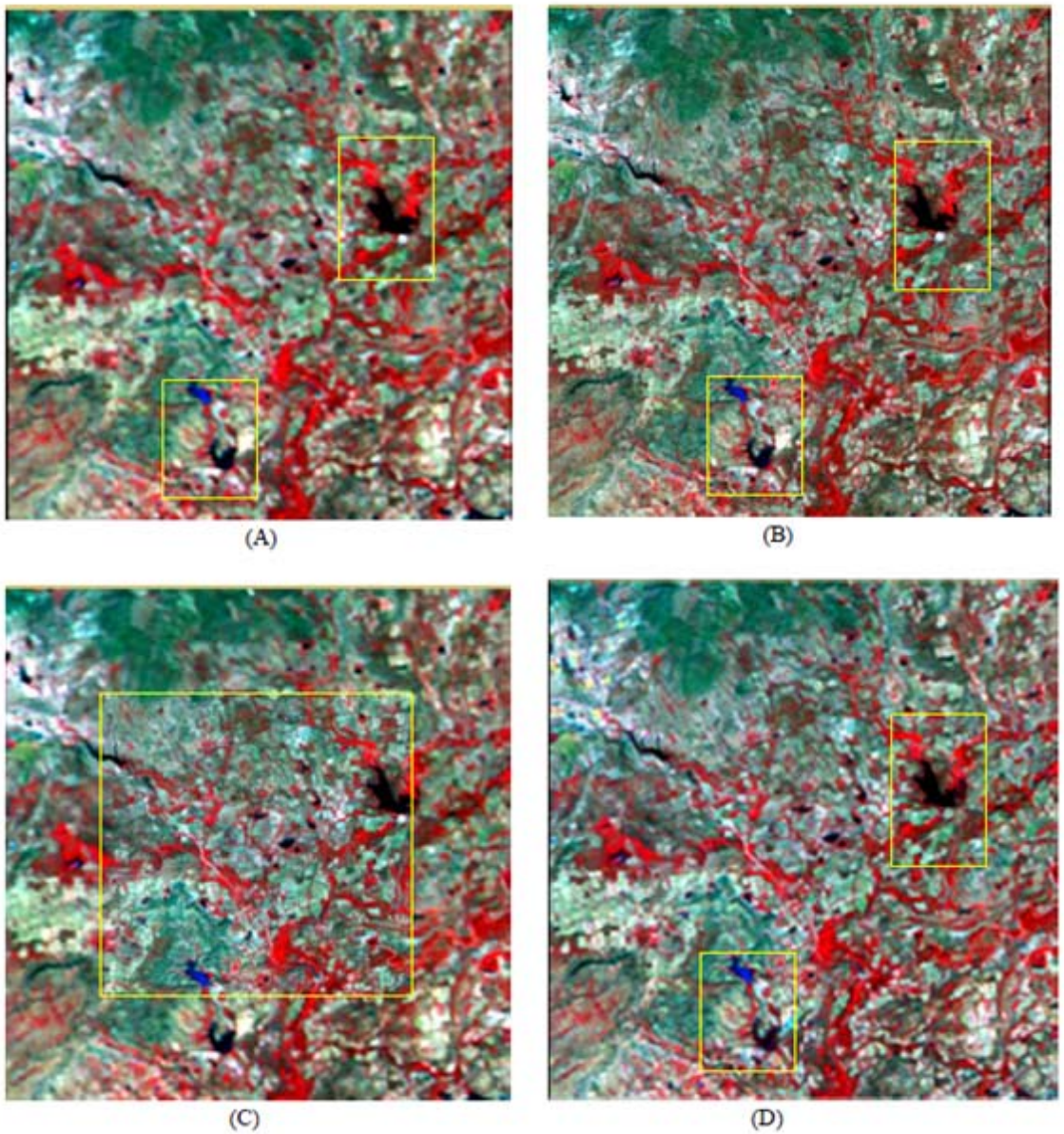


Figure 6: Synthetic LISS-III Images. (A) Full Scene of AWIFS Images. (B) Full Scene of LISS-III Image. (C) LISS-III at Centre of AWIFS Image. (D) Predicted LISS-III Image.

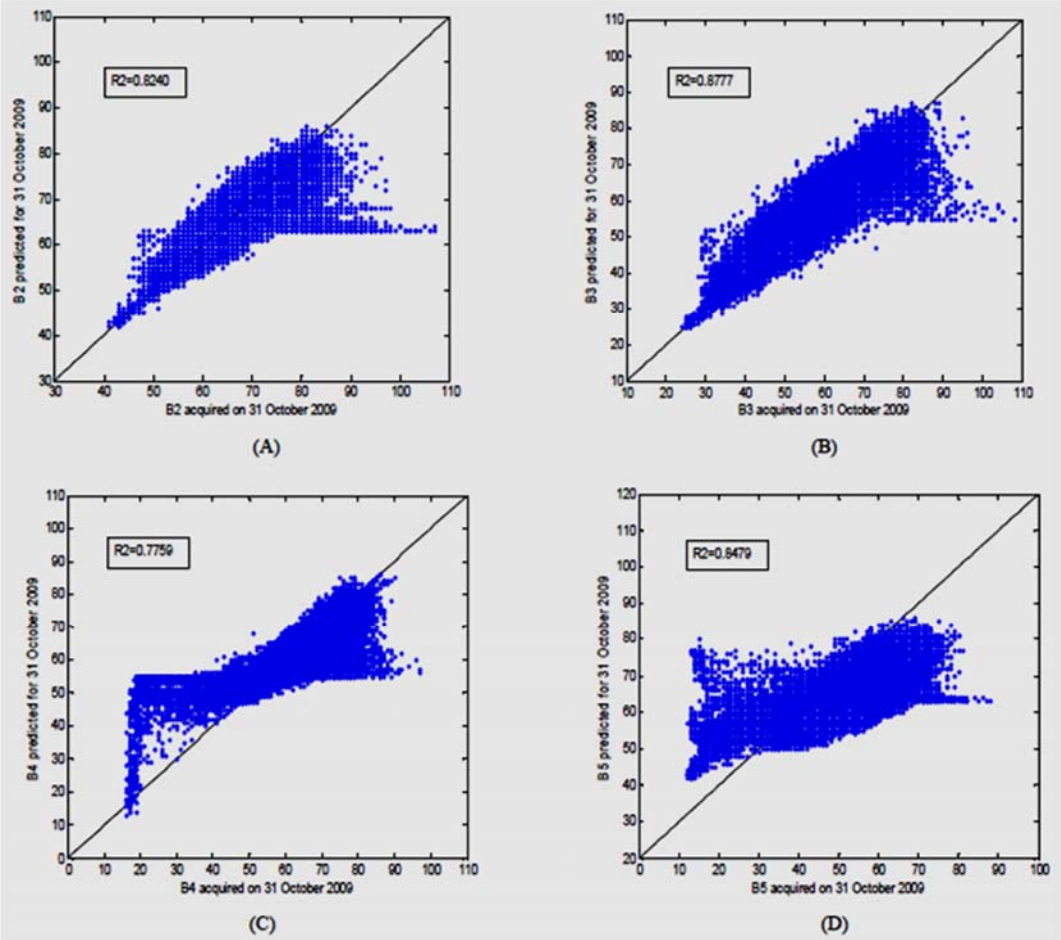


Figure 7: Scatter Plots Of Datasets.

TABLE II. QUALITY ASSESSMENT PARAMETERS.

| | | SSIM | RMSE | CC | ERGAS | SAM (º) |
|---|---|---|---|---|---|---|
| **Dataset I** | **B2** | 0.9489 | 3.1741 | 0.9032 | 3.8848 | 3.0308 |
| | **B3** | 0.9302 | 4.4571 | | | |
| | **B4** | 0.9149 | 5.2757 | | | |
| | **B5** | 0.9422 | 3.6971 | | | |
| **Dataset II** | **B2** | 0.9674 | 2.3446 | 0.9430 | 2.0804 | 1.5519 |
| | **B3** | 0.9582 | 3.0940 | | | |
| | **B4** | 0.9627 | 2.9849 | | | |
| | **B5** | 0.9637 | 2.8689 | | | |

## REFERENCES

[1] Auernhammer, H. 2001. "Precision Farming—The Environmental Challenge." Computers and Electronics in Agriculture 30: 31–43. doi:10.1016/S0168-1699(00)00153-8.

[2] Sanyal, J., and X. X. Lu. 2004. "Application of Remote Sensing in Flood Management with Special Reference to Monsoon Asia: A Review." Natural Hazards 33: 283–301. doi:10.1023/B: NHAZ.0000037035.65105.95.

[3] Loew, A., R. Ludwig, and W. Mauser. 2006. "Derivation of Surface Soil Moisture from ENVISAT ASAR Wide Swath and Image Mode Data in Agricultural Areas." IEEE Transactions on Geoscience and Remote Sensing 44: 889–899. doi:10.1109/TGRS.2005.863858.

[4] Kerr, J. T., and M. Ostrovsky. 2003. "From Space to Species: Ecological Applications for Remote Sensing." Trends in Ecology and Evolution 18: 299–305. doi:10.1016/S0169-5347(03)00071-5.

[5] Gillespie, T. W., G. M. Foody, D. Rocchini, A. P. Giorgi, and S. Saatchi. 2008. "Measuring and Modelling Biodiversity from Space." Progress in Physical Geography 32: 203–221. doi:10.1177/0309133308093606.

[6] Coops, N. C., M. Johnson, M. A. Wulder, and J. C. White. 2006. "Assessment of QuickBird High Spatial Resolution Imagery to Detect Red Attack Damage Due to Mountain Pine Beetle

Infestation." Remote Sensing of Environment 103: 67–80. doi:10.1016/j.rse.2006.03.012.

[7] Jiji, C. V., and S. Chaudhuri. 2006. "Single-Frame Image Super-Resolution through Contourlet Learning." EURASIP Journal on Applied Signal Processing 2006: 235–235.

[8] Elad, M., and D. Datsenko. 2009. "Example-Based Regularization Deployed to Super-Resolution Reconstruction of a Single Image." The Computer Journal 52: 15–30. doi:10.1093/comjnl/ bxm008.

[9] Chang, H., D. Y. Yeung, and Y. Xiong. 2004. "Super-Resolution through Neighbor Embedding." Proceedings IEEE Conference CVPR 1: I-275–I-282.

[10] Freeman, W. T., T. R. Jones, and E. C. Pasztor. 2002. "Example-Based Superresolution." IEEE Computer Graphics and Applications 22: 56–65. doi:10.1109/38.988747.

[11] Baker, S., and T. Kanade. 2002. "Limits on Super-Resolution and How to Break Them." IEEE Transactions on Pattern Analysis and Machine Intelligence 24: 1167–1183. doi:10.1109/ TPAMI.2002.1033210.

[12] Islam, T., P. K. Srivastava, M. Gupta, X. Zhu, and S. Mukherjee. eds. 2014. Computational Intelligence Techniques in Earth and Environmental Sciences, 281. Dordrecht: Springer.

[13] Srivastava, P. K., D. Han, M. R. Ramirez, and T. Islam. 2013. "Machine Learning Techniques for Downscaling SMOS Satellite Soil Moisture Using MODIS Land Surface Temperature for Hydrological Application." Water Resources Management 27 (8): 3127–3144. doi:10.1007/ s11269-013-0337-9.

[14] Ni, K., and T. Q. Nguyen. 2007. "Image Super Resolution Using Support Vector Regression." IEEE Transactions on Image Processing 16: 1596–1610. doi:10.1109/TIP.2007.896644.

[15] Kim, K. I., D. H. Kim, and J. H. Kim. 2004. "Example-Based Learning for Image Super-Resolution," In Proc. 3rd Tsinghua-KAIST Joint Workshop Pattern Recognition, Beijing, December 16–17, 140–148.

[16] Gyanesh Chander, Michael J. Coan, Pasquale L. Scaramuzza. 2008 "Evaluation and Comparision of the IRS-P6 and the Landsat Sensors". IEEE Transactions on Geoscience and Remote Sensing, 209–221, Vol. 46, doi 10.1109/TGRS.2007.907426.

[17] Radhika, K.S.R., Rao, C.V., Kamakshi Prasad, V.: Enhancement of AWiFS Spatial Resolution with SVM Learning. In 6th International Advanced Computing Conference, 978-1-4673-8286-1/16 IEEE DOI 10.1109/IACC.2016.42, pp. 178-183 (2016).

[18] Huihui Song, Bo Huang. 2012 "Spatiotemporal Satellite Image Fusion Through One-Pair Image Learning". IEEE Transactions on Geoscience and Remote Sensing, 1-13, doi 10.1109/TGRS.2012.2213095.

[19] Bo Huang, Huihui Song. 2012 "Spatiotemporal Reflectance Fusion via Sparse Representation". IEEE Transactions on Geoscience and Remote Sensing, 3707-3715, Vol. 50, doi 10.1109/TGRS.2012.2186638.

[20] Wangmeng Zuo, David Zhang,Liang Lin, Yuchi Huang, DeyuMeng, Lei Zhang. 2017. "Distance Metric Learning via Iterated Support Vector Machines". IEEE Transactions on Image Processing, 4937-4949, Vol. 26, doi 10.1109/TIP.2017.2725578.

[21] Hankui Zhang, Bo Huang. 2013. "Support vector Regression-Based Down Scaling for Inter calibration of multi resolution satellite images". IEEE Transactions on Geoscience and Remote Sensing, 1114-1123, Vol. 51, doi 10.1109/TGRS.2013.2243736.

[22] Chih-Wei Hsu, Chih-Chung Chang, chih-Jen Lin. 2010. "A practical guide to support vector classification". http://www.csie.ntu.edu.tw/~cjlin.

[23] J. Malleswara Rao, C. V. Rao, A.Senthil Kumar, B.lakshmi, V.K. Dadhwal. 2015. "Spatio temporal Data Fusion using temporal High-pass modulation and Edge primitives". IEEE Transactions on Geoscience and Remote Sensing, 1-8, doi 10.1109/TGRS.2015.2422712.

[24] Gustavo Camps, Jose L. Rojo. 2006. "Robust support vector regression for biophysical variable estimation from Remotely Sensed Images". IEEE Transactions on Geoscience and Remote Sensing Letters, Vol. 3, 339-343, doi 10.1109/LGRS.2006.871748.

]25] Farid Melgani, Lorenzo Bruzzone. 2004. "Classification of Hyperspectral Remote Sensing Images with Support Vector Machines". IEEE Transactions on Geoscience and Remote Sensing, 1778-1790, Vol. 42, doi 10.1109/TGRS.2004.831865.

[26] Akpora Okujeni, Sebastian van der Linden, Benjamin Jakimow, Andreas Rabe, Jochen Verrelst, Patrick Hostert. 2014. "A Comparision of Advanced Regression Algorithms for Quantifying Urban Land Cover". Remote Sensing, 6, 6324-6346, doi:10.3390/rs6076324.

[27] Nello Cristianini, John Shawee-Taylor. 2000. "An Introduction to Support Vector Machines".

[28] Shigeo Abe. 2005. "Two-class Support Vector Machines".

[29] National Remote Sensing Centre, https://bhuvan.nrsc.gov.in.

[30] Majeed, A.S. "Eco-friendly design of flow injection system for the determination of bismarck brown R dye (2018)", International Journal of Pharmaceutical Research, 10 (3), pp. 399-408.

[31] Ch. Venkateswara Rao, P.Shasidhar Reddy, D. S. Jain, K. M. M. Rao. 2007. "Quantitative Value Addition Analysis of Multisensor Data Fusion". The Icfai Journal of Earth Sciences, Vol. 1, No. 1.